

Research Article

Neural grafts containing exosomes derived from Schwann cell-like cells promote peripheral nerve regeneration in rats

Taotao Hu^{1,2,†}, Shusen Chang^{1,2,†}, Fang Qi^{1,2}, Zhonghui Zhang^{1,2}, Jiayin Chen^{1,2}, Lingli Jiang^{1,2}, Dali Wang^{1,2}, Chengliang Deng^{1,2}, Kaiyu Nie^{1,2}, Guangchao Xu^{1,2,†,*} and Zairong Wei^{1,2,†,*}

¹Department of Burns and Plastic Surgery, Affiliated Hospital of Zunyi Medical University, No. 149 Dalian Road, Huichuan District, Zunyi, Guizhou 563003, China; and ²The Collaborative Innovation Center of Tissue Damage Repair and Regeneration Medicine of Zunyi medical University, No. 6 West Xuefu Road, Xinpu District, Zunyi, Guizhou, 563003, China

*Correspondence. Guangchao Xu, Email: Guangchao_Xu@zmu.edu.cn; Zairong Wei, Email: Zairongwei@sina.com

[†]These authors contributed equally to this work.

Received 5 August 2022; Revised 6 December 2022; Accepted 2 March 2023

Abstract

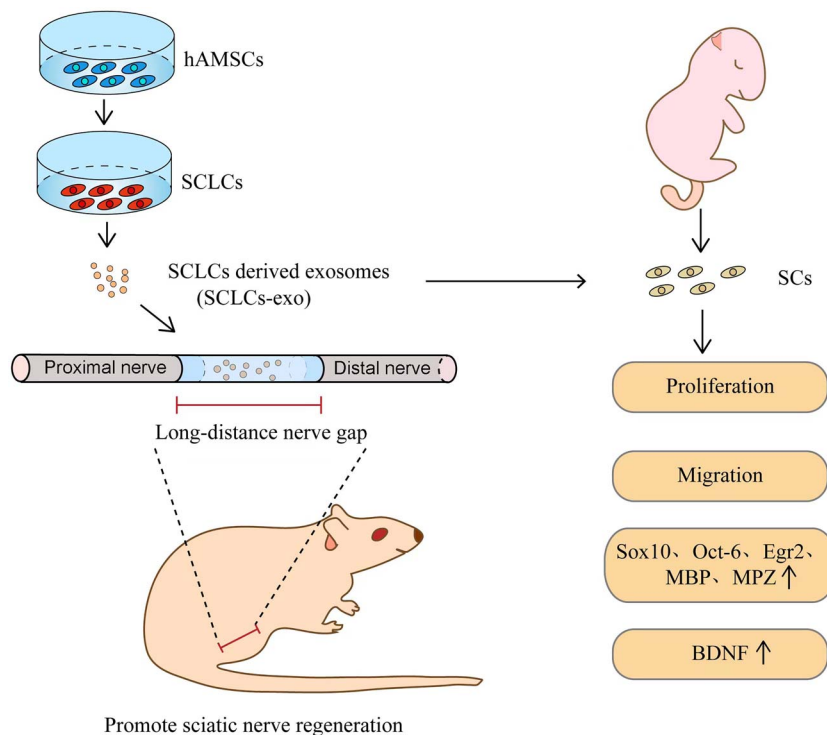
Background: Schwann cell-like cells (SCLCs), differentiated from mesenchymal stem cells, have shown promising outcomes in the treatment of peripheral nerve injuries in preclinical studies. However, certain clinical obstacles limit their application. Hence, the primary aim of this study was to investigate the role of exosomes derived from SCLCs (SCLCs-exo) in peripheral nerve regeneration.

Methods: SCLCs were differentiated from human amniotic mesenchymal stem cells (hAMSCs) *in vitro* and validated by immunofluorescence, real-time quantitative PCR and western blot analysis. Exosomes derived from hAMSCs (hAMSCs-exo) and SCLCs were isolated by ultracentrifugation and validated by nanoparticle tracking analysis, WB analysis and electron microscopy. A prefabricated nerve graft was used to deliver hAMSCs-exo or SCLCs-exo in an injured sciatic nerve rat model. The effects of hAMSCs-exo or SCLCs-exo on rat peripheral nerve injury (PNI) regeneration were determined based on the recovery of neurological function and histomorphometric variation. The effects of hAMSCs-exo or SCLCs-exo on Schwann cells were also determined via cell proliferation and migration assessment.

Results: SCLCs significantly expressed the Schwann cell markers glial fibrillary acidic protein and *S100*. Compared to hAMSCs-exo, SCLCs-exo significantly enhanced motor function recovery, attenuated gastrocnemius muscle atrophy and facilitated axonal regrowth, myelin formation and angiogenesis in the rat model. Furthermore, hAMSCs-exo and SCLCs-exo were efficiently absorbed by Schwann cells. However, compared to hAMSCs-exo, SCLCs-exo significantly promoted the proliferation and migration of Schwann cells. SCLCs-exo also significantly upregulated the expression of a glial cell-derived neurotrophic factor, myelin positive regulators (SRY-box transcription factor 10, early growth response protein 2 and organic cation/carnitine transporter 6) and myelin proteins (myelin basic protein and myelin protein zero) in Schwann cells.

Conclusions: These findings suggest that SCLCs-exo can more efficiently promote PNI regeneration than hAMSCs-exo and are a potentially novel therapeutic approach for treating PNI.

Graphical Abstract



Key words: Schwann cell-like cells, Exosomes, Peripheral nerve injury, Mesenchymal stem cells, Nerve regeneration

Highlights

- Exosomes derived from SCLCs serve as paracrine factors that regulate axon regeneration.
- SCLC-derived exosomes express Schwann cell markers and promote Schwann cell proliferation and migration.
- In a periphery nerve injury rat model, SCLC-derived exosomes attenuated gastrocnemius muscle atrophy and enhanced motor function recovery.
- SCLC-derived exosomes also facilitated axonal regrowth, myelin formation and angiogenesis.

Background

Peripheral nerve injury (PNI) is a common chronic clinical issue, typically caused by inflammation, tumors and trauma, accounting for 3–10% of systemic trauma [1]. In fact, ~200,000 trauma-induced PNIs are reported in the USA and 300,000 in Europe each year. Moreover, patients with PNIs often experience permanent sensory impairment and severe motor dysfunction of the affected limb [2].

For PNI, particularly cases involving severe neurological deficits, nerve autografts can achieve good results and are widely considered the gold standard for PNI therapy [3]. However, the disadvantages of nerve autografts, including lack of donor source, loss of function of the donor nerve, formation of painful neuroma and mismatching of sensory axons

with motor axons, limit their application [4]. The further development of nerve grafts should provide an alternative therapeutic strategy to achieve improved PNI regeneration effects [5]. Indeed, specific types of nerve grafts, such as nerve conduits, have been successfully applied to bridge sciatic nerve defects, yielding excellent therapeutic effects [6].

As an important component of the peripheral nervous system, Schwann cells contribute significantly to the regenerative capacity of peripheral nerves. After PNI, the loss of contact with axons by chevron cells triggers de-differentiation, leading to transformation from a myelin-forming to a repair cell phenotype. The latter removes fragmented axonal debris and degraded myelin and reuses it for myelin regeneration [7,8]. Moreover, de-differentiated Schwann cells produce and

secrete pro-inflammatory factors to recruit macrophages that accelerate the clearance of axonal and myelin debris [9,10]. Following de-differentiation, Schwann cells proliferate and extend longitudinally to form Büngner bands that help guide axon regeneration and secrete various cytokines, growth factors, neurotrophic factors and extracellular matrix molecules to promote neuronal survival and axon regeneration [10]. Hence, therapeutic strategies that combine Schwann cells with nerve conduits significantly promote PNI regeneration [11,12]. However, due to the difficulty in obtaining Schwann cells *in vitro*, as well as their poor proliferative capacity, the clinical application of Schwann cell transplantation for PNI treatment has been limited [13,14].

Stem cells, which have self-renewal and multidirectional differentiation potential, are now widely used as an alternative resource for Schwann cells [15,16]. Schwann cell-like cells (SCLCs) can be differentiated from mesenchymal stem cells and highly expressed Schwann cell markers, such as glial fibrillary acidic protein (GFAP) and S100 [16]. For example, mesenchymal stem cells (MSCs) derived from bone marrow [17,18], adipose [19,20], amniotic membrane [21], amniotic fluid [22], tonsils [23], dental pulp [24] and pluripotent stem cells [25] can differentiate into SCLCs, which have exhibited promising preclinical therapeutic potential for PNIs. However, various risks are associated with cell transplantation, including immune rejection and tumorigenicity, among others [26,27]. Nevertheless, the therapeutic effects of stem cell transplantation may be attributed to their paracrine effects [28,29]. In fact, exosomes, the main paracrine products of stem cells, can mediate cell-to-cell contact by transporting signaling molecules, such as bioactive proteins, lipids and nucleic acids [30]. In this way, exosomes can regulate various functions of recipient cells, including cytokine secretion, cell proliferation, apoptosis and migration [31]. Compared with stem cells, exosomes have the advantages of wide availability, easy storage, functional stability and low tumorigenesis risk [28]. Hence, nerve grafts comprising exosomes and nerve conduits may provide an efficient therapeutic strategy for PNIs.

While exosomes injected intravenously or directly into a nerve-injury site tend to be rapidly cleared from the body, continuous delivery at the injury site via a vehicle facilitates their maximum utilization [32,33]. Matrigel, also known as Englebreth-Holm-Swarm gel, is a mixture of extracellular factors extracted from Englebreth-Holm-Swarm mouse sarcomas. Matrigel is enriched with growth factors and extracellular proteins, including type IV collagen and laminin [34,35], and has good biocompatibility and physicochemical properties [36]. As such, it is widely used in tumor therapy and tissue engineering to construct slow-release systems for cells and drug delivery [37]. Silicone catheters, which are hollow devices made of biologically inert materials with high mechanical strength, stability and biocompatibility [38,39], are also widely used in the treatment of PNIs [40].

Previously, we reported that SCLCs induced by human amniotic mesenchymal stem cells (hAMSCs) exhibit superior effects for treating PNIs [21,41]. Hence, in the current study

we sought to investigate the role of SCLC-derived exosomes (SCLCs-exo) in PNI regeneration. To this end, SCLCs-exo were generated through ultracentrifugation; their purity was then assessed via electron microscopy, nanoparticle tracking analysis (NTA) and western blot (WB) analysis. Subsequently, SCLCs-exo were mixed with Matrigel and used to fill silicone tubes to construct nerve grafts, which were then applied to treat PNIs in an injured sciatic nerve rat model. After 6 weeks of observation, SCLCs-exo significantly promoted PNIs regeneration *in vivo*, as well as Schwann cell proliferation, migration and release of neurotrophic factors *in vitro*. Collectively, these findings suggest that the application of SCLCs-exo represents a potential therapeutic strategy for PNIs.

Methods

Extraction and identification of exosomes

Exosomal fetal bovine serum (FBS) was generated by centrifuging FBS at $100,000 \times g$ for 16 h, as described previously [42]. Exosomes were obtained from the supernatant of hAMSCs or SCLCs at $\sim 80\%$ confluence after replacing the complete medium with exosomal FBS for 24 h. The supernatants were then centrifuged at $300 \times g$ for 10 min, $2000 \times g$ for 10 min and $10,000 \times g$ for 30 min. Subsequently, exosomes were collected by ultracentrifugation at $100,000 \times g$ for 70 min, resuspended in phosphate-buffered saline (PBS) and stored at -80°C . Exosome morphology and size were examined using a transmission electron microscope and a nanoparticle tracking analyzer (ZetaView_Particle Metrix, Germany), respectively. Expression of exosome protein markers was determined via WB analysis using antibodies against CD9, CD63 and TSG101 (Abcam, USA).

Primary cell extraction and culture

This study was approved by the Biomedical Research Ethics Committee of the Affiliated Hospital Zunyi Medical University (approval number: KLLY-2020-037). hAMSCs were extracted using a previously published protocol with minor modifications [21]. Uncontaminated amniotic membranes separated by cesarean section were selected, rinsed with PBS and shredded. The amniotic membrane was digested with 0.05% trypsin-EDTA solution (CAS:9001-12-1, Solarbio, Beijing, China) containing 0.75% collagenase II (CAS:9002-07-7, Solarbio, Beijing, China) for 40 min. Cells were resuspended with Dulbecco's modified Eagle's medium (DMEM; 11885084, Gibco, USA) containing 10% FBS (1099-141C, Gibco, USA), 1% penicillin (P1400, Solarbio, Beijing, China) and 20 ng/ml basic fibroblast growth factor (450-33, Peprotech, USA) and then incubated at 37°C with 5% CO_2 . Third-generation hAMSCs were identified by flow cytometry and hAMSC lipogenic, osteogenic and chondrogenic differentiation kits (ChemBio, China) according to the manufacturer's instructions.

For the extraction of Schwann cells, the sciatic nerve was collected from Sprague Dawley (SD) rats on day 1 postnatal;

the outer membrane of the nerve was stripped microscopically and the nerve was then clipped [43]. The nerve was digested with 0.03% collagenase II (CAS:9002-07-7, Solarbio, Beijing, China) and 0.25% trypsin–EDTA solution (CAS:9001-12-1, Solarbio, Beijing, China) at 37°C for 25 min, with shaking every 5 min. Finally, the Schwann cells were seeded into culture dishes and incubated at 37°C with 5% CO₂.

Production of SCLCs

SCLCs were produced according to a previously published protocol with minor modifications [21]. Third-generation hAMSCs, at 80% confluence, were cultured for 24 h with DMEM low-sugar complete medium (11885084, Gibco, USA) containing 1 mM β -mercaptoethanol. The medium was then replaced with DMEM low-sugar complete medium containing 35 ng/ml all-*trans* retinoic acid (ATRA, R2625, Sigma, USA) and cultured for 72 h. The medium was then replaced with DMEM low-sugar complete medium containing 14 mmol/l forskolin (66575–29-9, Sigma, USA), 10 ng/ml basic fibroblast growth factor (AF-100-18B, PEPROTECH, USA), 5 ng/ml platelet-derived growth factor-aa (PDGF-AA, 07–1436, Sigma, USA) and 200 ng/ml heregulin (H7660, Sigma, USA) and cultured for 2 weeks. The medium was replaced every 3 days.

Cell proliferation and migration

Cell proliferation assays were performed using a 5-ethynyl-2-deoxyuridine (EdU) cell proliferation assay kit (R11053.9, RiboBio, Guangzhou, China) according to the manufacturer's instructions. Schwann cells were cultured in 96-well plates and spiked with 40 μ g/ml of hAMSCs-exo or SCLCs-exo or an equal volume of PBS. After 6 h, the cells were observed under an inverted fluorescence microscope (Olympus, Tokyo, Japan).

Cell migration experiments were performed using 8- μ m-pore Transwell migration chambers (Corning, NY, USA). A total of 2×10^5 Schwann cells in 200 μ l of serum-free medium were inoculated in the upper chamber of the Transwell plate. Subsequently, 40 μ g/ml of hAMSCs-exo or SCLCs-exo or an equal volume of PBS was added to the upper chamber, while the lower chamber was filled with complete medium. The plates were incubated for 24 h before removing non-migrated cells from the upper chamber with a cotton swab. The migrated cells were stained with 0.1% crystalline violet (Beyotime, Nantong, China) for 30 min, photographed and counted under a light microscope (Olympus, Tokyo, Japan).

Transmission electron microscopy observation

For the transmission electron microscopy (TEM) observation of regenerating nerve myelin, the middle portion of the nerve was cut into 70-nm ultrathin sections along the cross-section and placed on a copper groove grid. The samples were stained with lead citrate and UO₂ acetate and observed via TEM. Five samples were randomly selected for each group and three

fields of view were selected for each sample. The thickness and G-ratio of the myelin sheath were calculated using ImageJ software.

Flow cytometry

Third-generation hAMSCs were adjusted to a density of 1×10^7 cells/ml with PBS; flow-through tubes were filled with 100 μ l of cell suspension and incubated with antibodies against CD29, CD44, CD105, CD34, CD45 and HLA-DR for 30 min at 4°C. Cells incubated with PBS were used as a control. After incubation, cells were washed thrice with PBS and the cells were resuspended in 300 μ l of PBS and assessed via flow cytometry (Beckman coulter, CA, USA).

WB analysis

Total proteins were extracted from cells using high-efficiency radioimmunoprecipitation assay buffer lysis solution (R0010, Solarbio, China). Then, 20 μ g of proteins were separated by 10% sodium dodecyl sulfate polyacrylamide gel electrophoresis gel (PG112, Yamei, China) and transferred to a polyvinylidene difluoride membrane (Millipore, USA). After 30 min of blocking with 5% protein-free blocking solution (PS108, Yamei, China), the membranes were incubated overnight with primary antibodies against S100 (ab52642, Abcam, USA), GFAP (ab7260, Abcam, USA) and glyceraldehyde 3-phosphate dehydrogenase (GAPDH, ab8245, Abcam, USA). The membranes were then incubated with secondary antibodies (ab6721, Abcam, USA) for 2 h and exposed with a fully automated gel-imaging system (BIO-RAD, USA).

Quantitative real-time PCR

Total cellular RNA was extracted from cultured cells using a FastPure Cell/Tissue Total RNA Isolation Kit (RC101, Vazyme, Nanjing, China). cDNA synthesis was performed using HiScript[®] III RT SuperMix (R323–01, Vazyme) according to the manufacturer's instructions [44]. Finally, amplification reactions were performed using ChamQ Universal SYBR qPCR Master Mix (Q711–03, Vazyme, Nanjing, China). cDNA was amplified for 40 cycles using the QuantStudio[™] Design & Analysis Software real-time PCR system (ABI, USA). GAPDH was used as the reference gene, and the relative gene expression was calculated using the $2^{-\Delta\Delta C_t}$ method. The relevant primer sequences are provided in Table 1.

Detection of Matrigel-packed exosomes

Matrigel inside the silicone tube was dehydrated, crushed and coated with gold. The Matrigel microstructure was then observed using scanning electron microscopy (SEM). Exosomes were labeled with the exosomal dye PKH67 (UR52303, Umibio, China) according to the manufacturer's protocol. After centrifugation at $100,000 \times g$ for 70 min at 4°C, the labeled exosomes were encapsulated in Matrigel. The distribution of exosomes in Matrigel was assessed by confocal laser scanning microscopy (CLSM).

Table 1. Primer sequences

Primer name	Type	Sequence	Length
NRG1	Forward primer	AGAGCCTGTTAAGAACTCGC	21
	Reverse primer	GTCCACTTCCAATCTGTTAGCA	22
GAPDH	Forward primer	CTGGGCTACACTGAGCACC	19
	Reverse primer	AAGTGGTCGTTGAGGGCAATG	21
ERBB3	Forward primer	AAAAGGGCTATGAGACGCT	19
	Reverse primer	AGTTCCAAAGACGCCAGA	18
JUN	Forward primer	GGAGCCAACCAACGTGA	17
	Reverse primer	GTCCCCGCTTCAGTAACAA	19
NCAM1	Forward primer	CCAAGGAGAAATCAGCGT	18
	Reverse primer	CATCATCGTTCCACACCA	18
BDNF	Forward primer	CTCTGCTCTTTCTGCTGGA	19
	Reverse primer	TATCTGCCGCTGTGACC	17
GDNF	Forward primer	AGGGAAAGGTCGCAGAG	17
	Reverse primer	TCACAGGAACCGCTACAA	18
SOX10	Forward primer	CCTGACTGAGCTGGCAAA	18
	Reverse primer	TCCCACCCTACCCTTTTCT	19
EGR2	Forward primer	GGTTGCGACAGGAGGTT	17
	Reverse primer	GGATGTGAGTGGTGAGGTG	19
VEGF-A	Forward primer	TCTGGGCTCTTCTCTCTCC	19
	Reverse primer	CCCCTCTCCTCTCCTTCT	19
OCT6	Forward primer	TTCTCAAGTGTCCTCAACGCC	20
	Reverse primer	GGTCATGCGCTTCTCCTT	18
NGF	Forward primer	CCAAGCTCACCTCAGTGTC	19
	Reverse primer	GTACGGTCTGCCTGTACG	19
MBP	Forward primer	AAATCGGCTCACAAGGGA	18
	Reverse primer	GGATTCGGGAAGGCTGA	17
MPZ	Forward primer	GATGAGGTGGGGACCTTC	18
	Reverse primer	ACTATGTCCGGTGGGTTTT	19

Nerve graft preparation and rat sciatic nerve transection model establishment

Male SD rats (6–8 weeks old, 180–220 g) were purchased from Chongqing Tengxin Biotechnology Company and housed in the SPF-grade animal facility of Zunyi Medical University Animal Center. All animal experiments conformed to the national animal ethics-related regulations and were approved by the Ethics Committee of the First Affiliated Hospital of Zunyi Medical University (Ethics Review No. KLLY(A)-2020-023). Briefly, 24 SD rats were randomly divided into three groups ($n = 8/\text{group}$). The rats were anesthetized by intraperitoneal injection of 3% sodium pentobarbital solution (2.5 mg/100 g of body weight) and the left sciatic nerve was then exposed. A 3-mm-long sciatic nerve segment was excised, creating a 5-mm-long nerve defect after natural retraction. The prefabricated nerve graft was implanted into the nerve defect using a 9-0 nerve suture. Finally, the wounds were sutured and routine feeding was continued. The nerve grafts were prepared by combining hAMSCs-exo (hAMSCs-exo group), SCLCs-exo (SCLCs-exo group) or PBS (Control group) with Matrigel at a 1 : 1 volume ratio to form a 1 $\mu\text{g}/\mu\text{l}$ mixture, which was then injected into a commercial silicone conduit ($\phi 2 \times 3$ mm, length 12 mm, Shanghai, China), followed by incubation at 37°C for 30 min.

Walking-track analysis

As described previously [45], a narrow 8.2 cm wide and 42 cm long walkway with white paper underneath was constructed. Rats with pigmented feet traveled through the walkway, leaving footprints on the white paper. The sciatic function index (SFI) was calculated using the following equation:

$$\text{SFI} = -38.3 \times (\text{EPL} - \text{NPL})/\text{NPL} + 109.5 \times (\text{ETS} - \text{NTS})/\text{NTS} + 13.3 \times (\text{EIT} - \text{NIT})/\text{NIT} - 8.8,$$

where PL represents the distance from the heel to the third toe, TS is the distance from the first toe to the fifth toe, IT is the distance from the second to the fourth toe, E is the experimental side, and N is the normal side. An SFI of -100 indicates complete impairment, while an SFI of 0 indicates normal function. Weekly tests were performed by two observers outside this study from week 1 to week 6 post-surgery.

Immunohistochemistry and immunofluorescence

Rats were euthanized via sodium pentobarbital overdose, and the regenerated nerves were removed along with the entire silicone tube. For hematoxylin-eosin (HE) staining, the middle portion of the regenerated nerve was cross-sectionally sliced into 7- μm -thick sections using an ultrathin sectioning

machine. Sections were stained using an HE staining kit (Solarbio, China). For toluidine blue (TB) staining, the middle portion of the regenerated nerve was cross-sectionally sliced into 1- μm -thick sections and stained with TB solution. For each group of five samples, the density of myelinated nerve fibers was calculated using NIH ImageJ software.

Cultured cells or tissue sections were sequentially fixed with 4% paraformaldehyde for 30 min, incubated with 0.1% Triton X-100 for 10 min and incubated with 5% bovine serum albumin for 30 min. The samples were then incubated with the corresponding primary antibodies overnight at 4°C and subsequently rinsed and incubated with the corresponding secondary antibodies at room temperature for 2 h. Finally, the samples were stained with the nuclear stain 4',6-diamidino-2-phenylindole (DAPI) for 5 min and photographed using an ortho-fluorescence microscope.

Wet weight and histological evaluation of the gastrocnemius muscle

After the rats were euthanized, the gastrocnemius muscles on both sides were stripped and their wet weight was measured with an electronic scale. The muscles from all eight rats in each group were weighed. Five rat gastrocnemius muscles were randomly selected from each group, fixed with 4% paraformaldehyde, paraffin-embedded and cut into 10- μm -thick slices along the cross-section. After dewaxing, they were stained using a Masson trichrome staining kit (Solarbio, China). Images of the muscle tissue were captured microscopically and five random fields of view were selected for each group. Muscle fiber diameter was measured using Image J software.

Exosome uptake experiment

To determine whether exosomes were internalized by Schwann cells, exosomes were labeled with PKH67 (UR52303, Umibio, China) according to the manufacturer's protocol. Exosomes labeled with PKH67 at a concentration of 40 $\mu\text{g}/\text{ml}$ were incubated with Schwann cells and observed under a laser confocal microscope (Carl Zeiss, Germany).

Statistical analysis

GraphPad Prism software (version 9.0) was used for graphing and statistical analysis. All data obeyed a normal distribution. Two samples were compared using the independent samples t-test, whereas comparisons involving three sample groups were performed using one-way ANOVA. The least significant difference test was used for homogeneity of variance and Dunnett's test was used for non-homogeneity of variance. Two-way ANOVA was used to analyze differences in SFI values over six consecutive weeks between the control, hAMSCs-exo and SCLCs-exo groups. All data are presented as mean \pm standard error of the mean; $p < 0.05$ was considered statistically significant.

Results

Production and identification of hAMSCs-exo and SCLCs-exo

As hAMSCs are a type of MSC, they express MSC surface-specific antigen markers. P3 generation hAMSCs were identified by flow cytometry, immunofluorescence and differentiation capacity. The results revealed that hAMSCs

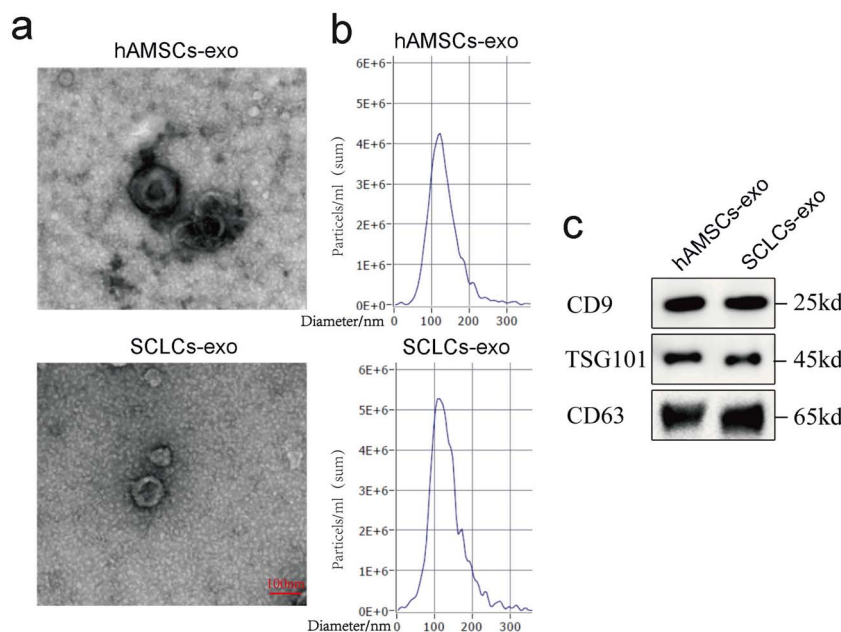


Figure 1. Identification of hAMSCs-exo and SCLCs-exo. (a) TEM analysis of hAMSCs-exo and SCLCs-exo morphology. Scale bar: 100 nm. Top: hAMSCs-exo; bottom: SCLCs-exo. (b) NTA determination of hAMSCs-exo and SCLCs-exo particle size; a single-peak pattern is observed (top: hAMSCs-exo; bottom: SCLCs-exo). (c) WB analysis of exosomal surface marker (CD9, CD63 and TSG101) expression. hAMSCs-exo human amniotic mesenchymal stem cells exosomes, SCLCs-exo Schwann cell-like cells exosomes, NTA nanoparticle tracking analyzer, WB western blot, CD9 cluster of differentiation 9, TSG101 tumor susceptibility 101

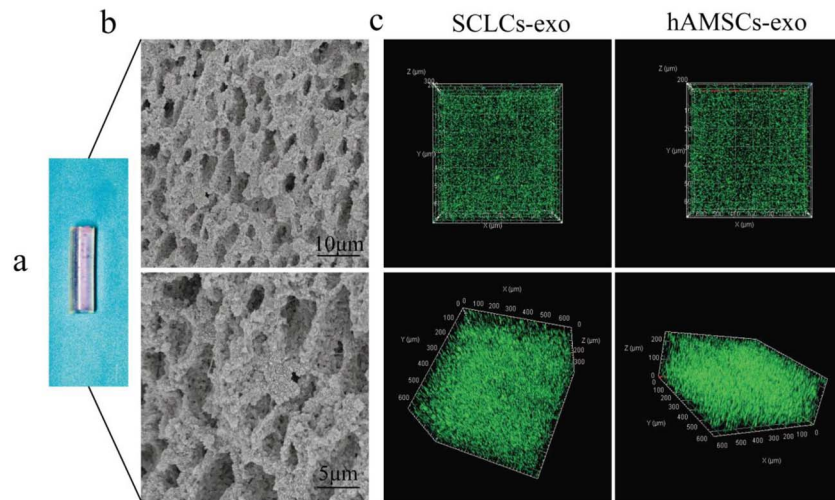


Figure 2. Characterization of neural graft material. (a) Gross observation of nerve grafts with exosomes encapsulated in Matrigel filling silicone tubes. (b) Characterization of Matrigel under SEM (low magnification, scale bar: 10 μm ; high magnification, scale bar: 5 μm). (c) Distribution of SCLCs-exo and hAMSCs-exo in Matrigel observed under confocal laser scanning microscopy. *hAMSCs-exo* human amniotic mesenchymal stem cells exosomes, *SCLCs-exo* Schwann cell-like cells exosomes, *SEM* scanning electron microscopy

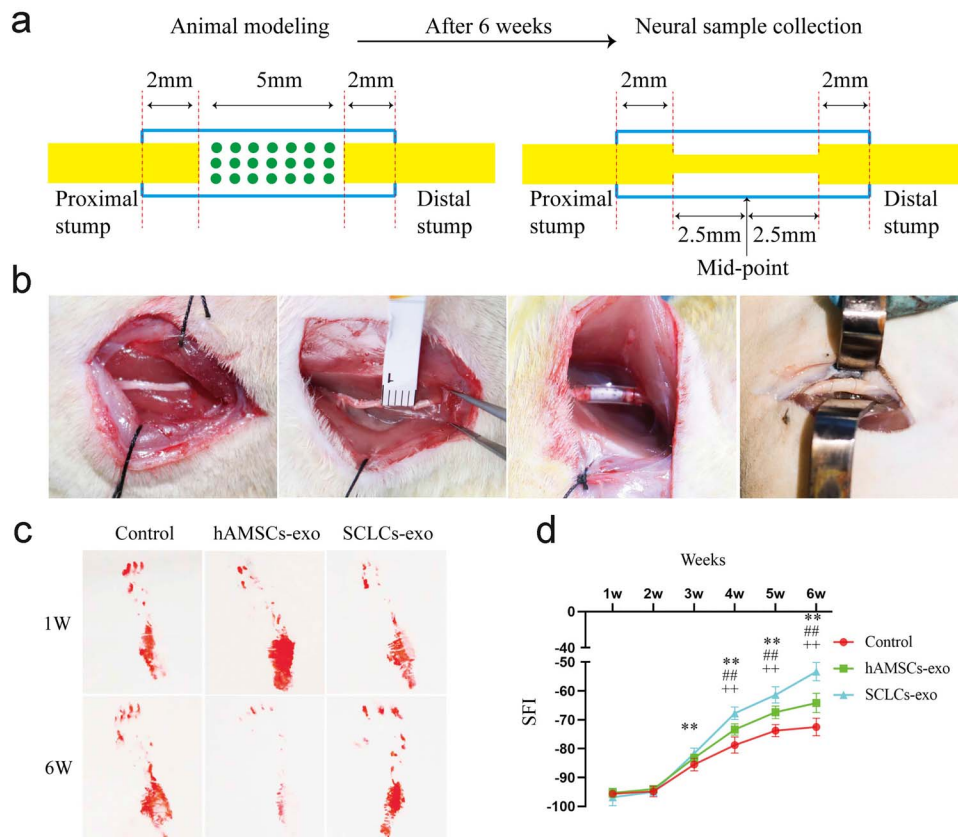


Figure 3. Assessment of neurological functional recovery in rats. (a) Schematic diagram of the anastomosis of the nerve graft to the transected sciatic nerve and of the regenerated nerve taken at week 6 post-surgery. (b) Isolation of the sciatic nerve, transection, suturing to the nerve graft and observation of the regenerated nerve in the silicone tube at week 6 post-surgery. (c) Representative footprints of rats in each group at weeks 1 and 6 post-surgery; (d) Statistical analysis of SFI values of the rats in each group from week 1 to week 6 post-surgery (n = 5/group; ** $p < 0.01$, SCLCs-exo vs control; ## $p < 0.01$, SCLCs-exo vs hAMSCs-exo; +++ $p < 0.01$, hAMSCs-exo vs control). *hAMSCs-exo* human amniotic mesenchymal stem cells exosomes, *SCLCs-exo* Schwann cell-like cells exosomes, *SFI* sciatic function index

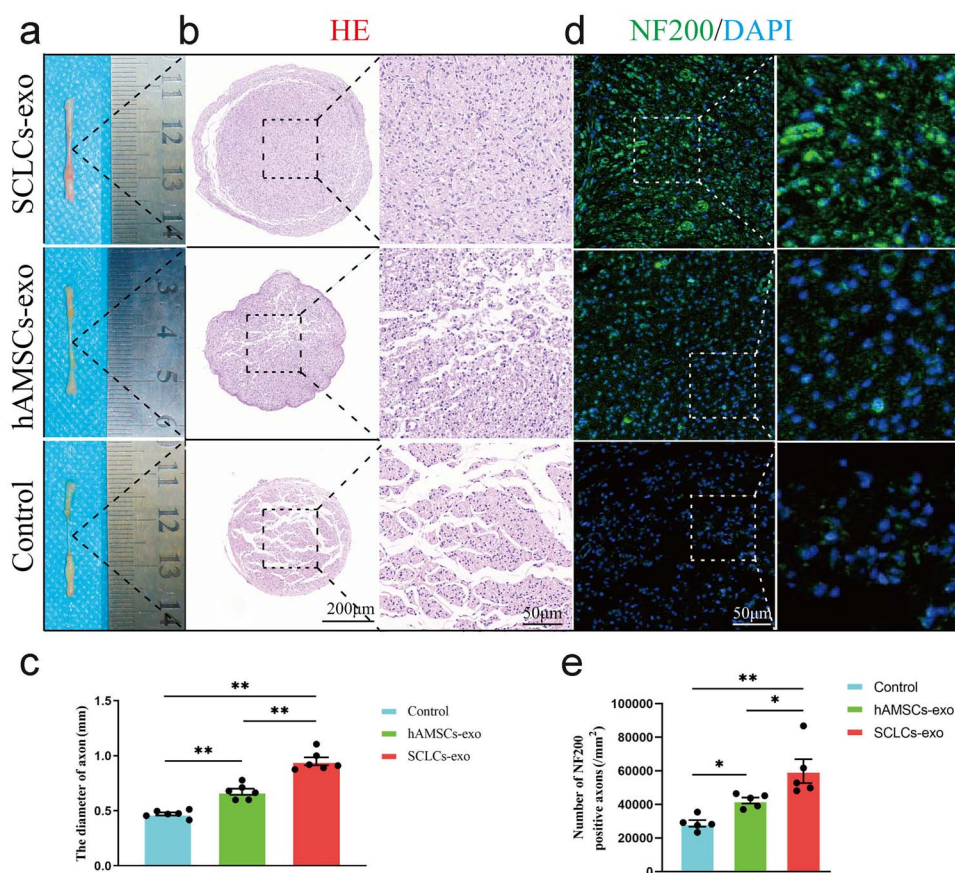


Figure 4. Morphological assessment of regenerating axons. (a) Representative images of regenerated sciatic nerve morphology from rats in each group. (b) HE-stained images of regenerated axons and 40× magnification. (c) Diameter of the regenerated nerves of the rats in each group ($n = 6$, $**p < 0.01$). (d) NF200 immunofluorescent stained images of regenerated axons and local 4× magnification. (e) NF200-positive axon density statistics ($n = 5$, $*p < 0.05$, $**p < 0.01$). *hAMSCs-exo* human amniotic mesenchymal stem cells exosomes, *SCLCs-exo* Schwann cell-like cells exosomes, *HE* hematoxylin–eosin, *NF200* neurofilament 200

positively expressed CD29 (99.6%), CD44 (99.8%) and CD105 (99.8%), but negatively expressed CD34 (0.2%), CD45 (0.1%) and HLA-DR (0.0%; [Figure S1a](#), see online [supplementary material](#)). *hAMSCs* also positively expressed the MSC surface marker vimentin but did not express CK19, a surface marker of amniotic epithelial cells ([Figure S1b](#), see online [supplementary material](#)). Furthermore, *hAMSCs* efficiently demonstrated osteogenic, lipogenic and chondrogenic differentiation capacity *in vitro* ([Figure S1c](#), see online [supplementary material](#)).

P3 generation *hAMSCs* were successfully induced into *SCLCs*, as immunofluorescence results revealed that *SCLCs* highly expressed the Schwann cell-specific surface markers S100 and GFAP ([Figure S2a](#), see online [supplementary material](#)). Moreover, *SCLC* morphology changed from long shuttle-shaped to oval with bipolar or multiple poles, resembling that of normal Schwann cells ([Figure S2b](#), see online [supplementary material](#)). WB and qPCR analyses further revealed that the Schwann cell surface markers GFAP and S100 were significantly upregulated in *SCLCs* ([Figure S2c–e](#), see online [supplementary material](#)).

After exosomes were extracted from *hAMSCs* and *SCLCs* through ultracentrifugation, we identified *hAMSCs-exo* and *SCLCs-exo* by TEM, NTA and WB analysis. TEM observation showed that both *hAMSCs-exo* and *SCLCs-exo* had a cup-shaped morphology ([Figure 1a](#)). Through NTA analysis, we found that the sizes of *hAMSCs-exo* and *SCLCs-exo* were mainly distributed in the range 30–150 nm, which is consistent with the expected exosome particle size range ([Figure 1b](#)). Exosomal surface markers, such as CD9, CD63 and TSG101, were also highly expressed in both *hAMSCs-exo* and *SCLCs-exo* ([Figure 1c](#)).

SCLCs-exo are uniformly encapsulated in Matrigel

To efficiently deliver exosomes to the site of nerve injury and provide biocompatible extracellular matrix, we encapsulated exosomes with Matrigel ([Figure 2a](#)). The Matrigel was observed under SEM as a porous and sparse 3D structure ([Figure 2b](#)). Under CLSM, PKH67-labeled *hAMSCs-exo* and *SCLCs-exo* were observed to be homogeneously suspended in the Matrigel at a high density ([Figure 2c](#)).

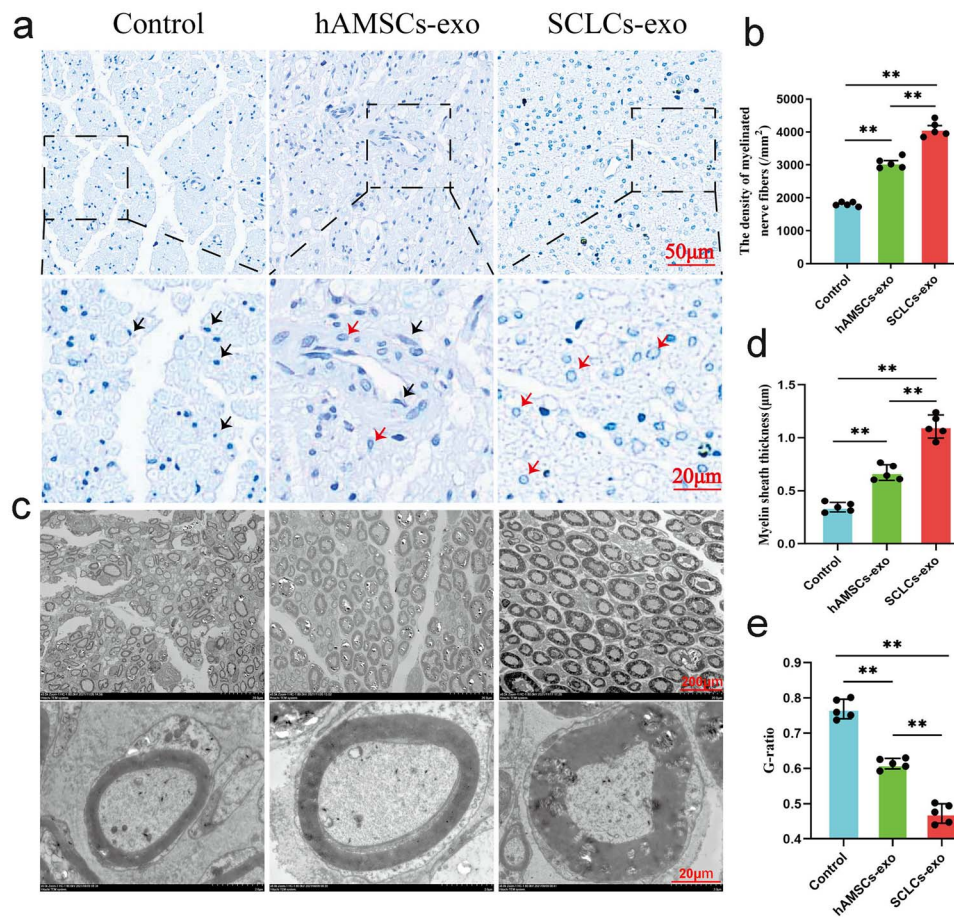


Figure 5. Regeneration of nerve myelin in rats of each group. (a) Representative images of sciatic nerves in rats stained with toluidine blue week 6 post-surgery. Top: low magnification, scale bar: 50 μm ; bottom: high magnification, scale bar: 20 μm ; red arrows: complete myelin sheath; black arrows: incomplete myelin sheath). (b) Statistics of myelin density based on toluidine blue staining ($n = 5$; $**p < 0.01$). (c) Representative TEM images of sciatic nerves in rats at week 6 post-surgery. Top: low magnification, scale bar: 20 μm ; bottom: high magnification, scale bar: 2 μm . Myelin thickness (d) and myelin G-ratio (e) measured and analyzed with Image J software ($n = 5$; $**p < 0.01$). *hAMSCs-exo* human amniotic mesenchymal stem cells exosomes, *SCLCs-exo* Schwann cell-like cells exosomes, *TEM* transmission electron microscopy

SCLCs-exo significantly promote functional recovery of injured sciatic nerves in rats

To evaluate the effects of SCLCs-exo in PNI regeneration, nerve grafts comprising silicone catheters and Matrigel-coated SCLCs-exo were used to treat PNI in a rat model with bridging 5-mm-long sciatic nerve defects (Figure 3a, b). Gait analysis was performed from week 1 to week 6 post-operatively to assess the recovery of motor function in the injured hind limb. Due to the sciatic nerve injury, the SFI values in all three groups of rats reached ~ 100 post-operatively (Figure 3c). However, a slightly increasing trend was observed in SFI values for each group from the third week onward. At weeks 4, 5 and 6, the SFI values in the SCLCs-exo group were significantly higher than those in the hAMSCs-exo or control groups; the SFI values in the hAMSCs-exo group were also significantly higher than those of the control group (Figure 3d). Our results indicated that SCLCs-exo could significantly promote the recovery of neurological function.

SCLCs-exo significantly promote axonal regeneration of injured sciatic nerves in rats

At week 6 post-surgery, the regenerated sciatic nerve was dissected from the silicone tubes in the rats of each group. The regenerated nerve was found to be thick in the SCLCs-exo group and thin in the hAMSCs-exo and control groups (Figure 4a). At week 6 post-surgery, HE staining confirmed that the sciatic nerve diameter of the rats in the SCLCs-exo group was thicker than that of rats in the hAMSCs-exo or control groups (Figure 4b, c). Moreover, the regenerated nerve fibers in the rats of the SCLCs-exo group were evenly arranged and dense, with an outer nerve membrane thicker than that of the hAMSCs-exo or control groups. In contrast, in the hAMSCs-exo and control groups, the regenerated nerve fibers were loosely arranged, the nerve bundles were widely spaced, the morphology was disorganized and the outer nerve membrane was incomplete (Figure 4b, c). To further characterize axonal regeneration, we performed neurofilament 200 (NF200) immunofluorescence

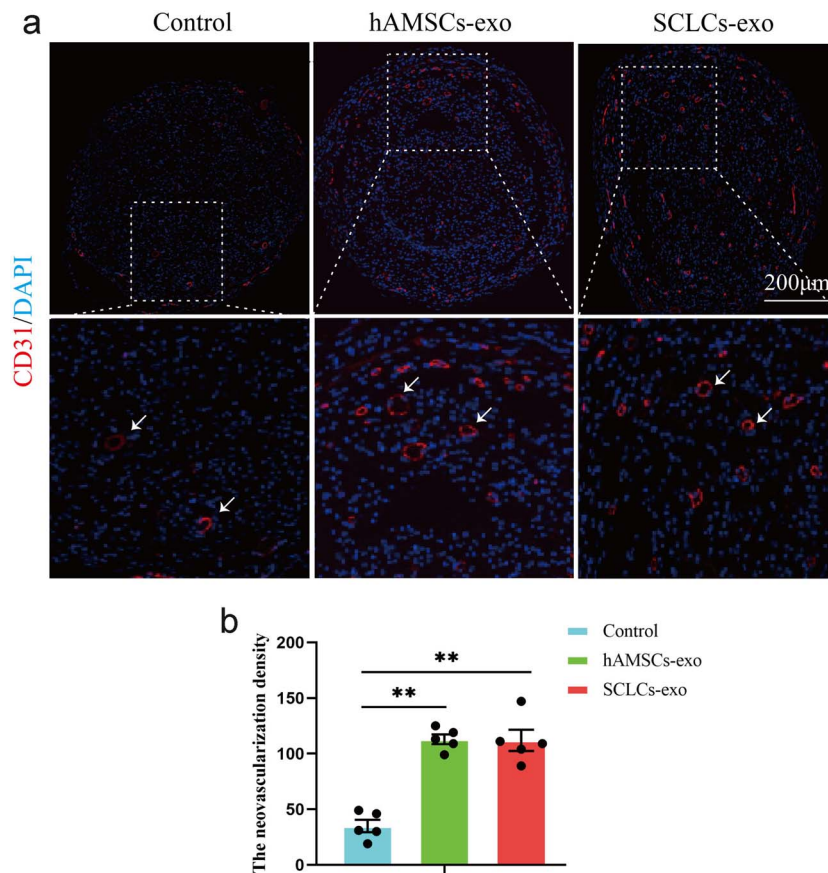


Figure 6. Observed angiogenesis of regenerating nerves. (a) CD31 immunofluorescent staining of regenerating sciatic nerve midpoint cross-sections in each group at week 6 post-surgery. White arrows: stained blood vessels. (b) Statistical analysis of vessel density based on positive CD31 staining in regenerative nerve tissue in each group ($n = 5/\text{group}$, $**p < 0.01$). *hAMSCs-exo* human amniotic mesenchymal stem cells exosomes, *SCLCs-exo* Schwann cell-like cells exosomes, *CD31* platelet endothelial cell adhesion molecule-1, *DAPI* 4',6-diamidino-2-phenylindole

staining of the regenerated sciatic nerves in rats 6 weeks post-surgery (Figure 4d). We observed that the number of NF-200-positive axons in the rats of the SCLCs-exo group were significantly higher than that of the control or hAMSCs-exo groups (Figure 4e).

SCLCs-exo significantly promote myelin formation of injured sciatic nerves in rats

To further characterize the effects of SCLCs-exo on injured sciatic nerves, TB staining was used to evaluate myelin formation. At week 6 post-surgery, the rats in the SCLCs-exo group had more myelinated nerve fibers with a uniform distribution than the control or hAMSCs-exo groups (Figure 5a). Moreover, the regenerated myelinated nerve-fiber density was significantly higher in the SCLCs-exo group compared with the control or hAMSCs-exo groups (4090.00 ± 104.09 , 1809.97 ± 28.65 and $3057.79 \pm 73.90/\text{mm}^2$, respectively; Figure 5b). To further characterize the myelin regeneration of sciatic nerves, we observed the regenerated nerve myelin in the rats of each group by TEM at week 6 post-surgery. The regenerated nerve myelin in the SCLCs-exo group was thicker

($1.12 \pm 0.03 \mu\text{m}$) than that of the control ($0.34 \pm 0.01 \mu\text{m}$) or hAMSCs-exo ($0.65 \pm 0.03 \mu\text{m}$) groups, with a regular morphology and neat arrangement (Figure 5c, d).

The G-ratio of myelin is commonly used to quantify regenerated myelin, where a high G-ratio indicates poor myelin formation. The G-ratio of regenerated myelin in the SCLCs-exo group was significantly lower than that of the control or hAMSCs-exo groups (Figure 5e).

SCLCs-exo significantly promote angiogenesis of injured sciatic nerves in rats

CD31, also known as PECAM-1, is a key blood-vessel marker [46]. Considering that neovascularization is essential for nerve regeneration [46], at 6 weeks post-surgery we performed CD31 immunofluorescence staining of the neonatal nerves for rats in each group (Figure 6a). Significantly more CD31-positive cells were observed in the SCLCs-exo and hAMSCs-exo groups compared with the control group. All CD31-positive cells in the single axon cross-sections of regenerated nerve sections from each group, in the low-magnification view, were counted (five samples per group).

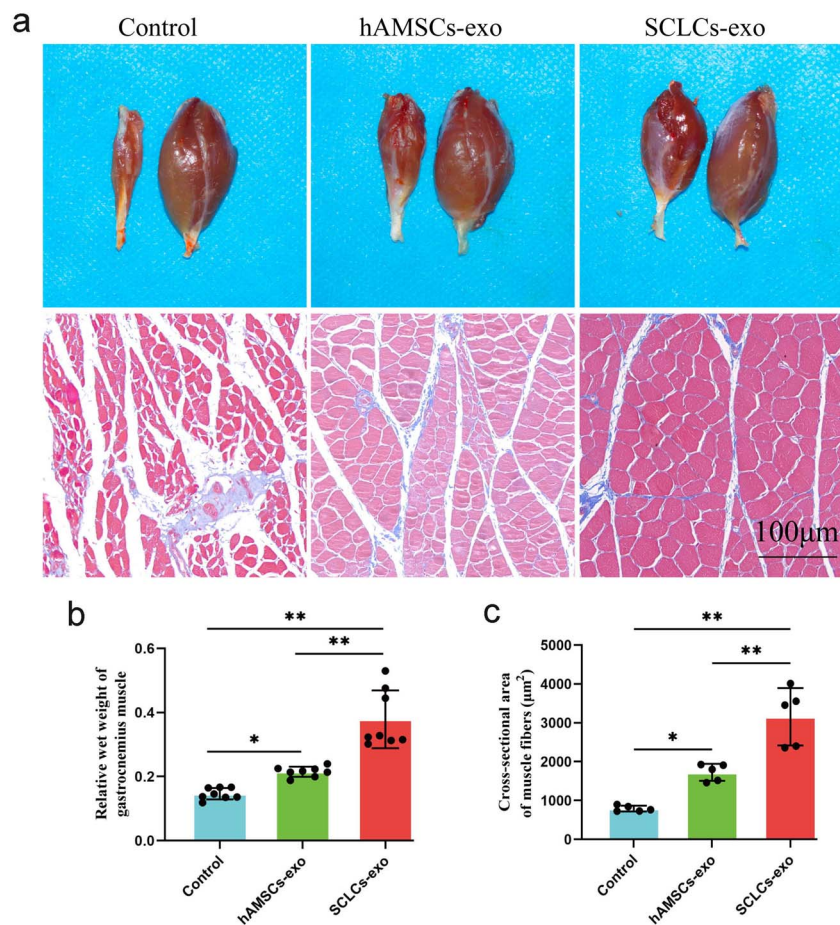


Figure 7. Gastrocnemius muscle assessment in rats. (a) Top: observation of hind limb gastrocnemius muscle in rats; bottom: representative Masson staining images of gastrocnemius muscles (scale bar: 100 μm). (b) Statistics of gastrocnemius muscle wet weight ratio in the rats of each group ($n = 8/\text{group}$; * $p < 0.05$, ** $p < 0.01$). (c) Statistical analysis of the mean cross-sectional area of individual muscle fibers ($n = 5$; * $p < 0.05$, ** $p < 0.01$). *hAMSCs-exo* human amniotic mesenchymal stem cells exosomes, *SCLCs-exo* Schwann cell-like cells exosomes

The neovascular density was significantly higher in the SCLCs-exo and hAMSCs-exo groups compared with the control group; however, the SCLCs-exo and hAMSCs-exo groups had comparable effects on promoting neurovascular regeneration (Figure 6b). These data suggested that SCLCs-exo significantly promoted angiogenesis of the injured sciatic nerve in rats.

SCLCs-exo significantly reduce the atrophy rate of denervated gastrocnemius muscles in rats

At week 6 post-surgery, the gastrocnemius muscles of both hind limbs were dissected from each rat. The gastrocnemius muscles from rats of the SCLCs-exo group exhibited no obvious atrophy, with their appearance found to be similar to that of normal gastrocnemius tissues. In contrast, in the control and hAMSCs-exo groups, the gastrocnemius muscles showed severe atrophy (Figure 7a). Moreover, the wet weight of the gastrocnemius muscles in the rats of the SCLCs-exo group was significantly heavier than that of the control or hAMSCs groups (Figure 7b). Using Masson staining to evaluate the midpoint cross-sections of the gastrocnemius

muscles in each rat, the gastrocnemius muscles of the rats in the SCLCs-exo group were observed to have the thickest and densest muscle fibers with minimal collagen intervals, while in the control or hAMSCs-exo groups, the muscle fibers were thinned with collagen growth (Figure 7a). The cross-sectional area of individual muscle fibers was statistically calculated for each group, and those of the SCLCs-exo group were much higher than those of the control or hAMSCs-exo groups (3157 ± 329.9 , 1724 ± 97.86 and $793.3 \pm 32.98 \mu\text{m}^2$, respectively; Figure 7c).

SCLCs-exo promote the proliferation and migration of Schwann cells *in vitro*

Schwann cells are the key cell population associated with PNI regeneration [46]. Hence, to evaluate the effects of SCLCs-exo on Schwann cells, primary Schwann cells were isolated from rats and assessed for expression of the surface marker S100 by immunofluorescent staining (Figure S3, see online supplementary material). After co-culturing PKH67-labeled hAMSCs-exo or SCLCs-exo with Schwann cells for 6 h, hAMSCs-exo and SCLCs-exo

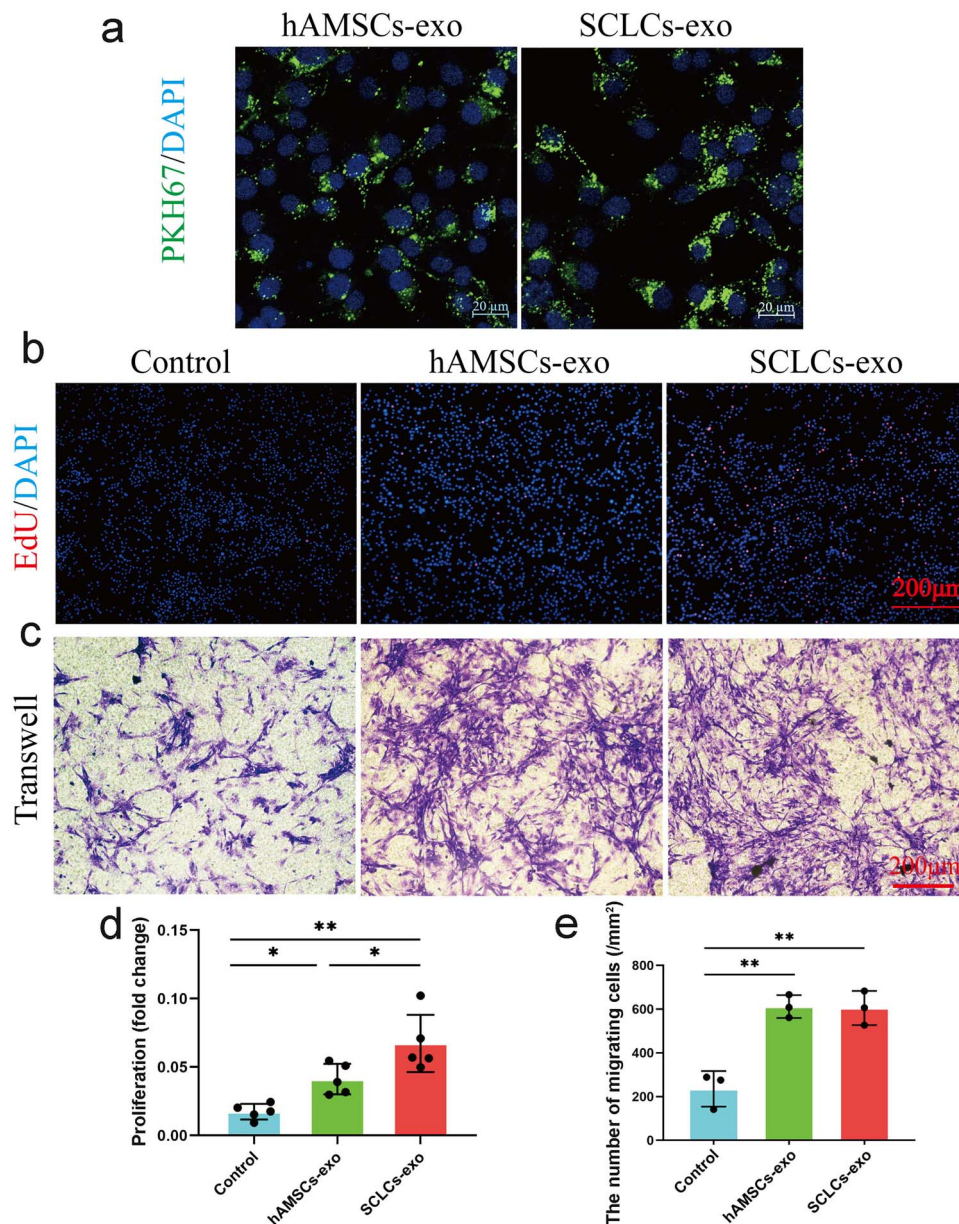


Figure 8. Effects of SCLCs-exo on the proliferation and migration of Schwann cells *in vitro*. (a) Confocal laser scanning microscopy observation of Schwann cells that have absorbed hAMSCs-exo and SCLCs-exo (scale bar: 20 μm). (b) Proliferation of Schwann cells following incubation with 40 $\mu\text{g}/\text{ml}$ of hAMSCs-exo, SCLCs-exo or an equivalent amount of PBS for 6 h (red represents cells that are proliferating; DAPI stains the nuclei blue; scale bar: 200 μm). (c) Schwann cell migration following incubation with 40 $\mu\text{g}/\text{ml}$ of hAMSCs-exo, SCLCs-exo or an equivalent amount of PBS for 24 h (scale bar: 200 μm). (d) Statistics of EdU positivity rate ($n = 3/\text{group}$; * $p < 0.05$, ** $p < 0.01$). (e) Quantitative analysis of Schwann cells migration ($n = 3/\text{group}$; ** $p < 0.01$). hAMSCs-exo human amniotic mesenchymal stem cells exosomes, SCLCs-exo Schwann cell-like cells exosomes, PBS phosphate-buffered saline, EdU 5-ethynyl-2-deoxyuridine, DAPI 4',6-diamidino-2-phenylindole

were both absorbed by Schwann cells and enriched around the nucleus, as evidenced by CLSM (Figure 8a). We then investigated the effects of SCLCs-exo on Schwann cell proliferation and migration. After co-incubation of hAMSCs-exo or SCLCs-exo with Schwann cells for 6 h, significantly more EdU-positive cells were detected in the SCLCs-exo group compared with the control or hAMSCs-exo group (Figure 8b); after co-incubating hAMSCs-exo or SCLCs-exo with Schwann cells for 24 h, more cells migrated across the Transwell membrane in the hAMSCs-exo and

SCLCs-exo groups compared with the control group (Figure 8c).

Next, a Transwell assay was employed to assess the effect of SCLCs-exo on Schwann cell migration. After co-incubating hAMSCs-exo or SCLCs-exo with Schwann cells for 24 h, more cells migrated across the membrane in the hAMSCs-exo and SCLCs-exo groups compared with the control group (Figure 8c). Statistical analysis showed more EdU-positive cells were also observed in the hAMSCs-exo group compared with the control group (Figure 8d); and the number

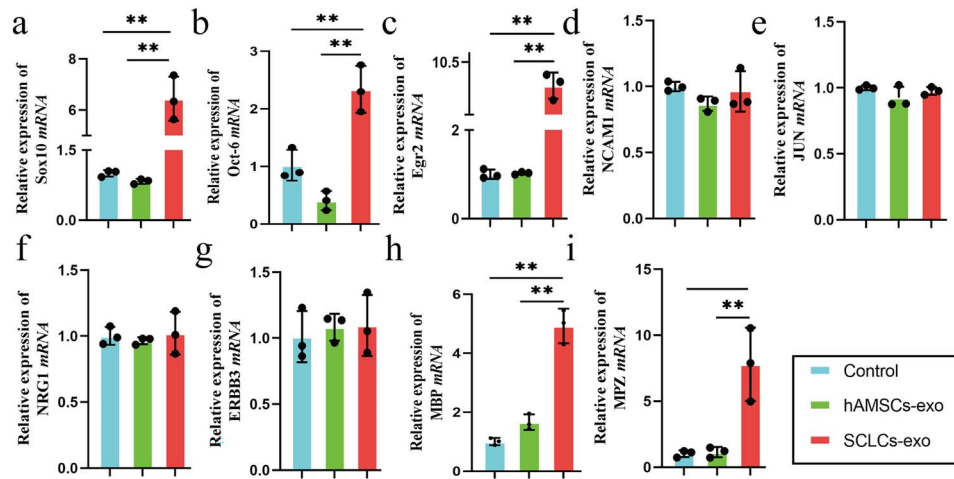


Figure 9. Myelin-related gene expression in Schwann cells incubated with SCLCs-exo. (a–i) Relative expression of *Sox10*, *Oct-6*, *Egr2*, *NCAM1*, *JUN*, *NRG1*, *ERBB3*, *MBP* and *MPZ* mRNA in Schwann cells following *in vitro* uptake of SCLCs-exo or hAMSCs-exo. PBS-treated cells were used as the control ($n = 3/\text{group}$; $**p < 0.01$). Expression levels were normalized against those of *GAPDH*. *Sox10* SRY-box transcription factor 10, *Oct-6* organic cation/carnitine transporter 6, *Egr2* early growth response protein 2, *NCAM1* neural cell adhesion molecule 1, *JUN* Jun proto-oncogene, *NRG1* neuroregulin1, *ERBB3* Erb-b2 receptor tyrosine kinase 3, *MBP* myelin basic protein, *MPZ* myelin and protein zero, *GAPDH* glyceraldehyde-3-phosphate dehydrogenase, *PBS* phosphate-buffered saline

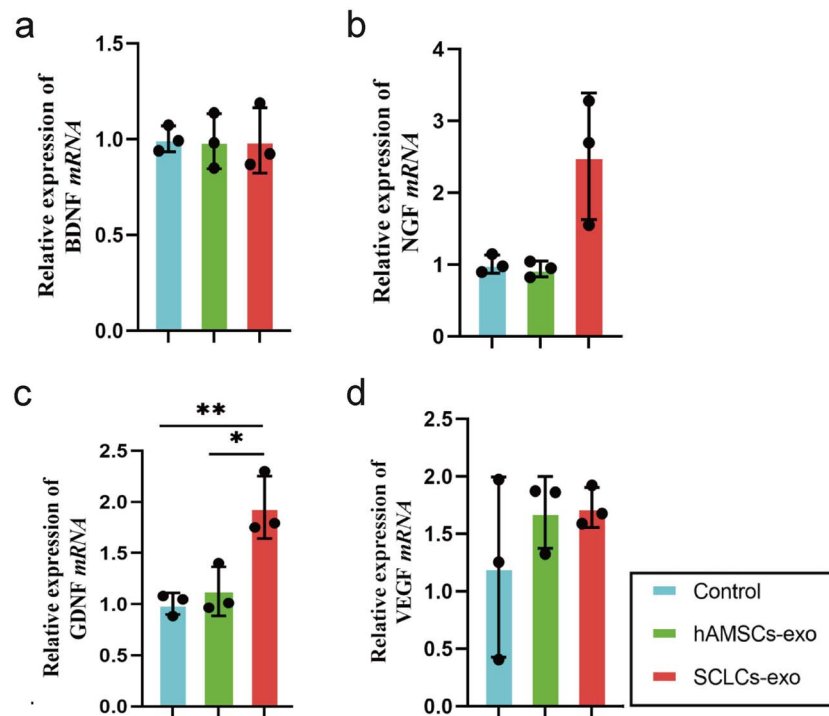


Figure 10. Evaluation of neurotrophic factors in Schwann cells stimulated by SCLCs-exo. (a–d) Relative expression of *BDNF*, *NGF*, *GDNF* and *VEGF* mRNA in Schwann cells after *in vitro* uptake of SCLCs-exo, hAMSCs-exo or PBS ($n = 3/\text{group}$; $*p < 0.05$, $**p < 0.01$). Expression levels were normalized against those of *GAPDH*. *BDNF* Brain-derived neurotrophic factor, *NGF* nerve growth factor, *GDNF* glial cell line-derived neurotrophic factor, *VEGF* vascular endothelial growth factor, *GAPDH* glyceraldehyde-3-phosphate dehydrogenase.

of Schwann cells that crossed the membrane per unit area revealed 605.3 ± 45.13 , 612.1 ± 30.15 and 235.6 ± 47.08 cells/ mm^2 in the SCLCs-exo group, hAMSCs-exo group and the control group, respectively (Figure 8e).

SCLCs-exo promote the expression of myelin-positive regulatory genes in Schwann cells SRY-box transcription factor 10 (*SOX10*), organic cation/carnitine transporter 6 (*OCT-6*), early growth response protein

2 (*EGR2*), neuroregulin1 (*NRG1*), Erb-b2 receptor tyrosine kinase 3 (*ERBB3*), Jun proto-oncogene (*JUN*), neural cell adhesion molecule 1 (*NCAM1*), myelin basic protein (*MBP*) and myelin and protein zero (*MPZ*) are common genes expressed by Schwann cells and are closely related to peripheral nerve myelin formation and maintenance [47]. After co-incubating hAMSCs-exo or SCLCs-exo with Schwann cells, qPCR was used to determine the mRNA levels of these genes. The myelin regulatory genes *SOX10*, *OCT-6* and *EGR2*, and the myelin proteins *MBP* and *MPZ* were significantly up-regulated in the SCLCs-exo group compared with the hAMSCs-exo group (Figure 9).

SCLCs-exo promote the expression of neurotrophic factors in Schwann cells

Nerve growth factor (NGF), brain-derived neurotrophic factor (BDNF) and GDNF are the main neurotrophic factors secreted by Schwann cells and contribute to nerve regeneration and repair [48]. Moreover, vascular endothelial growth factor A (VEGF-A) is a common factor that promotes vascular regeneration and is secreted by Schwann cells to promote the vascular regeneration of peripheral nerves [46]. Therefore, we assessed the mRNA expression of these factors in Schwann cells following incubation with SCLCs-exo. SCLCs-exo promoted the expression of *GDNF* and *NGF*, but not *BDNF* (Figure 10). Moreover, *GDNF* was significantly up-regulated in the SCLCs-exo group compared with the control or hAMSCs-exo groups (Figure 10). Both hAMSCs-exo and SCLCs-exo failed to promote *VEGF-A* expression in Schwann cells.

Discussion

This study is the first to investigate the function of hAMSC-derived SCLCs-exo in PNI regeneration in a rat sciatic nerve transection model. In this study, SCLCs were derived from hAMSCs *in vitro*, and the exosomes of hAMSCs and SCLCs were isolated by differential centrifugation. Immediately thereafter, animal experiments were conducted to further confirm the pro-neural regenerative function of hAMSCs-exo and SCLCs-exo. SCLCs-exo were found to promote the functional recovery of sciatic nerves in a superior manner to hAMSCs-exo. Further morphological observations of the regenerated nerves revealed that SCLCs-exo significantly promoted axonal growth, myelin formation and angiogenesis. Although the axonal regeneration and myelin formation of rats in the hAMSCs-exo group were inferior to those in the SCLCs-exo group, their pro-vascular regenerative capacity was comparable and their overall pro-neural regenerative effect was superior to that of the control group. Similarly, Ching *et al.* reported that exosomes derived from Schwann cell-like differentiated adipose stem cells at a concentration of 1 $\mu\text{g}/\mu\text{l}$ promoted axonal growth in cultured neurons *in vitro*; however, complementary *in vivo* studies were not performed to confirm the promotive effect on neural regeneration [20]. Meanwhile, Chen *et al.*

reported that exosomes from human adipose-derived stem cells at a concentration of 1 $\mu\text{g}/\mu\text{l}$ promoted the regeneration of transected sciatic nerves in rats. However, their study evaluated nerve regeneration outcomes only in terms of the number of regenerated axons, myelination and recovery of atrophied gastrocnemius muscle [49]. Additionally, Yu *et al.* found that injecting exosomes from skin-derived precursor Schwann cells (2×10^{10} exosomes in 16 μl of PBS) with Matrigel, at a 1 : 1 volume ratio, into nerve grafts made from commercial silicone catheters significantly promoted the recovery of motor, sensory and electrophysiological functions, while also promoting axonal growth, myelin formation and recovery of atrophied gastrocnemius muscles in a rat sciatic nerve transection model [50]. Thus, the more comprehensive assessment of regenerated nerves in Yu *et al.*'s study is consistent with our findings in promoting the regeneration of transected sciatic nerves in rats. Furthermore, a study by Lopez-Leal *et al.* revealed that Schwann cell-derived exosomes promote axonal regeneration by mediating neuron–glia communication [51]. Similarly, a study by Lopez-Verrilli *et al.* reported that Schwann cell-derived exosomes can promote axonal regeneration by communicating with neighboring axons [43]. Although our findings suggest that SCLCs-exo have similar pro-neural regenerative effects to Schwann cell exosomes, we were unable to provide an in-depth investigation of this mechanism. Hence, given that previous studies have defined the specific components of Schwann cell exosomes [52], further investigation is warranted to ascertain whether SCLCs-exo have similar components.

In this study, we used Matrigel-filled silicone tubes as a carrier for exosomes as the systemic administration of exosomes is limited by rapid clearance from the organism, thereby reducing the exosomal action efficiency. Therefore, the topical delivery of exosomes encapsulated in the Matrigel may enhance their ability to repair PNIs. Matrigel is a hydrogel with a morphology that is affected by temperature, such that it is a liquid at 4°C but forms a cross-linked solid network via polymerization at 37°C, thus allowing it to simulate an *in vivo* 3D microenvironment [53]. Indeed, many studies have reported the use of Matrigel as a suitable carrier for exosomes in nerve regeneration. For example, encapsulation of human adipose stem cell-derived exosomes in Matrigel effectively improves PNI regeneration [49]. Meanwhile, Matrigel co-transplantation with Schwann cells in spinal cord hemisections and complete transection models of nerve injuries, enhances the survival and migration of Schwann cells [54,55]. By transplanting exosomes from skin-derived precursor Schwann cells encapsulated in Matrigel into rat sciatic nerve defects, a slow-release system was previously generated, and nerve regeneration was significantly promoted [50]. In fact, SKP-SC-Evs are efficiently released from Matrigel and taken up by nerve cells proximal and distal to the injured sciatic nerve, with fluorescently labeled exosome particles consistently accumulating around the injured nerve. Herein, we observed that Matrigel is a sparse gel with

porosity that allows good exosome attachment. CLSM results further revealed that hAMSCs-exo and SCLCs-exo were uniformly distributed in the Matrigel. Based on these results, we developed artificial nerve grafts by filling silicone tubes with Matrigel-coated SCLCs-exo and confirming the promotion of PNI regeneration in a rat sciatic nerve transection model.

Exosomes exert biological roles in myriad ways, such as activating cell-surface receptors by delivering ligands, including proteins and lipids, or by directly delivering their contents, such as proteins or RNA, into recipient cells [41]. As such, the key to our SCLCs-exo exerting their pro-neural regenerative effects may be their internalization by recipient cells. Indeed, previous studies have demonstrated that exosomes derived from SCLCs, via stem cell-induced differentiation, can be internalized by Schwann cells in injured nerves, thereby regulating the function of Schwann cells and promoting nerve regeneration [49,50]. Therefore, to further understand the mechanism by which SCLCs-exo promotes neural regeneration, we conducted *in vitro* experiments on the Schwann cell uptake of SCLCs-exo. Using the exosomal dye PKH67, labeled hAMSCs-exo or SCLCs-exo were co-cultured with, and taken up by, Schwann cells. Both hAMSCs-exo and SCLCs-exo were concentrated around the nucleus, confirming that Schwann cells internalize hAMSCs-exo and SCLCs-exo. Following PNI, mature Schwann cells dedifferentiate, proliferate, migrate and form Büngner bands, which become axonal regeneration channels [56,57]. Therefore, we further evaluated whether the proliferation and migration capacity of Schwann cells changed following internalization of exosomes. Using EdU and Transwell assays, we confirmed that, although hAMSCs-exo and SCLCs-exo both promoted the proliferation and migration of Schwann cells, the proliferative effect elicited by SCLCs-exo was stronger. This is consistent with the observation by Chen *et al.* who reported that ASC-Exos promote Schwann cell proliferation and migration [49]. However, the underlying mechanisms remain unclear.

In vivo, we observed a significant myelin regeneration capacity of nerves in the SCLCs-exo group rats. That is, we first examined the expression of pro-myelinogenesis genes following the Schwann cell internalization of exosomes. *SOX10*, *EGR2*, *OCT-6*, *NRG1*, *ERBB3*, *NCAM1* and *JUN* are common myelin regulators, whereas *MBP* and *MPZ* are associated with myelin formation [47]. We found that SCLCs-exo promoted the expression of *SOX10*, *EGR2*, *OCT-6*, *MBP* and *MPZ* in Schwann cells.

After nerve injury, dedifferentiated Schwann cells secrete various neurotrophic factors, including *NGF*, *BDNF* and *GDNF*, to form a microenvironment conducive to axon growth, axon regeneration and myelin formation [58,59]. Therefore, we further examined the expression of *NGF*, *BDNF* and *GDNF* following internalization of exosomes by Schwann cells. SCLCs-exo promoted the expression of *GDNF* in Schwann cells but not *NGF* or *BDNF*. Meanwhile, hAMSCs-exo did not alter the expression of *BDNF*, *NGF* nor *BDNF* in Schwann cells. However, this is not consistent

with the findings of Chen *et al.* [49]. This discrepancy may be caused by the differential regulation of neurotrophic factors by SCLCs-exo and hAMSCs-exo, although this theory requires further investigation.

Angiogenesis is also particularly important during reinnervation as it initiates nerve regeneration; VEGF-A is a key biological factor in angiogenesis [60,61]. Along with secreting neurotrophic factors, Schwann cells secrete VEGF-A [46], which promotes neurovascular development and maturation and has the potential to protect motor and sensory neurons. Moreover, VEGF-A is thought to protect Schwann cells and promote their proliferation and migration [62]. *In vivo*, we also observed the pro-neuroangiogenic effects of hAMSCs-exo and SCLCs-exo. Therefore, we further assessed the expression of *VEGF-A* mRNA following internalization of exosomes by Schwann cells. Neither hAMSCs-exo nor SCLCs-exo were found to significantly impact *VEGFA* expression. This is inconsistent with the pro-neuroangiogenic phenomenon observed in the pathological sections of nascent nerves in the rats of the hAMSCs-exo and SCLCs-exo groups. We speculate that this may be due to the effect of other pro-angiogenic factors. Alternatively, SCLCs-exo and hAMSCs-exo may have been taken up by other cells besides Schwann cells. Therefore, we suggest that the SCLCs-exo promotion of PNI regeneration may be related to its induced expression of pro-neural factors. Meanwhile, the pro-neural regenerative ability of hAMSCs-exo may be attributed to their pro-Schwann cell proliferative and migratory abilities. However, further research is required to determine whether hAMSCs-exo or SCLCs-exo are internalized by cells other than Schwann cells, such as macrophages or neuronal cells.

This study had certain limitations. First, we did not conduct a controlled study using autologous nerve grafts or commercial synthetic catheters. As autologous nerve grafts are considered the gold standard for treating PNIs, it is essential to further improve the efficacy of our fabricated nerve grafts prior to comparison. We used exosomes of hAMSCs, the source cells of induced SCLCs, as a control, along with simple PBS and Matrigel-filled nerve grafts constructed from silicone tubes. Although the role of MSCs and their exosomes in PNI regeneration has been demonstrated, the role of hAMSC-derived exosomes in PNI regeneration remains unknown. If the pro-PNI regeneration effect of hAMSCs-exo is better than that of SCLCs-exo, then there is no need to induce the differentiation of hAMSCs into SCLCs. However, our study confirmed that the pro-neural regenerative effect of SCLCs-exo was greater than that of hAMSCs-exo. Therefore, in future work, we will further optimize our prefabricated nerve grafts and compare them with autologous nerve grafts. Second, our experimental design involved a shorter 5-mm nerve gap as we deemed it was more important to achieve reliable nerve regeneration in a shorter nerve gap than less reliable results in a longer and more challenging gap. We have demonstrated that our fabricated nerve grafts can significantly promote regeneration of 5-mm long sciatic nerve defects in rats. In future experiments, we will investigate

regeneration in nerve defects with longer gaps and use larger animal models.

Conclusions

Our findings suggest that the integration of exosomes from hAMSC-derived SCLCs into neural grafts represents a promising paradigm for PNI regeneration. We successfully generated nerve grafts by encapsulating SCLCs-exo in Matrigel, which was used to fill silicone tubes to bridge 5-mm-long sciatic nerve defects in rats. Nerve grafts containing SCLCs-exo significantly promoted the functional recovery of the sciatic nerves, attenuated atrophy of the innervated gastrocnemius muscle, and promoted axonal growth and myelin formation. Moreover, SCLCs-exo, when internalized by Schwann cells, promoted Schwann cell proliferation, migration, myelin formation and secretion of neurotrophic factors. Although this is postulated to represent the main mechanism for promoting neural regeneration, the specific molecular mechanism underlying this phenomenon requires further exploration.

Abbreviations

ANOVA: Analysis of variance; ASC-Exos: Exosomes from human adipose-derived stem cells; BDNF: Brain-derived neurotrophic factor; CD9: Cluster of differentiation 9; CLSM: Confocal laser scanning microscopy; DMEM: Dulbecco's modified Eagle's medium; EDTA: Ethylene Diamine Tetraacetic Acid; EdU: 5-Ethynyl-2-deoxyuridine; EGR2: Early growth response protein 2; ERBB3: Erb-b2 receptor tyrosine kinase 3; FBS: Fetal bovine serum; GAPDH: Glyceraldehyde-3-phosphate dehydrogenase; GDNF: Glial cell-derived neurotrophic factor; GFAP: Glial fibrillary acidic protein; hAMSCs: Human amniotic mesenchymal stem cells; hAMSCs-exo: Exosomes derived from hAMSCs; HE: hematoxylin-eosin; HLA-DR: Human Leukocyte Antigen DR; JUN: Jun proto-oncogene; MBP: Myelin basic protein; MPZ: Myelin and protein zero; NCAM1: Neural cell adhesion molecule 1; NF200: neurofilament 200; NGF: Nerve growth factor; NRG1: Neuregulin1; OCT-6: Organic cation/carnitine transporter 6; PBS: Phosphate-buffered saline; PNI: Peripheral nerve injury; qPCR: Real-time Quantitative PCR Detecting System; SCLCs: Schwann cell-like cells; SCLCS-exo: Exosomes derived from SCLCs; SD: Sprague Dawley; SEM: Scanning electron microscopy; SFI: Sciatic function index; SKPSC-Evs: Exosomes from skin-derived precursor Schwann cells; Sox10: SRY-box transcription factor 10; SPF: Specific Pathogen Free; TB: Toluidine blue; TEM: Transmission electron microscopy; TSG101: Tumor susceptibility 101; VEGF: Vascular endothelial growth factor; WB: Western blot.

Acknowledgments

We thank Zhi Xiao (Key Laboratory of Brain Science, Zunyi Medical University, No. 6 West Xuefu Road, Xinqu District, Zunyi, Guizhou,

563000, China) for technical support. We would like to thank Editage (www.editage.cn) for English language editing.

Supplementary data

Supplementary data is available at *Burns & Trauma Journal* online.

Funding

This work was financially supported by the Innovation Group Major Research Project of Guizhou Province Education Department (No. Qianjiaohe KY [2017]043), the Science and Technology Support Project of Guizhou Province (2020-5012), the PhD Fund of Scientific Research Foundation of the Affiliated Hospital of Zunyi Medical University (2020-03), the National Nature Science Foundation of China (81660325) and the Collaborative Innovation Center of the Chinese Ministry of Education (2020-39), the Master Fund of Scientific Research Foundation of the Affiliated Hospital of Zunyi Medical University (2016-35).

Authors' contributions

TH: Conceptualization, investigation, methodology and writing of the original draft. SC: Conceptualization, investigation and methodology. FQ: Investigation and methodology. DW: Investigation and resources. CD and KN: Investigation. ZZ, JC, and LJ: Methodology. GX: Resources, supervision, validation and writing—review and editing. ZW: Resources, supervision, validation and funding acquisition.

Ethics approval and consent to participate

The study involving human participants was reviewed and approved by the Biomedical Research Ethics Committee of the First Affiliated Hospital of Zunyi Medical University, Grant No. KLLY-2020-037. Participants provided written informed consent. Experiments involving animals complied with national regulations related to animal ethics and were approved by the Ethics Committee of the Affiliated Hospital of Zunyi Medical University, Ethics Review No. KLLY(A)-2020-023.

Competing interests

None declared.

Data availability

The data used in this publication are available upon request.

References

- Gu X, Ding F, Yang Y, Liu J. Construction of tissue engineered nerve grafts and their application in peripheral nerve regeneration. *Prog Neurobiol.* 2011;93:204–30.
- Lee JH, Roy J, Sohn HM, Cheong M, Liu J, Stammers AT, et al. Magnesium in a polyethylene glycol formulation provides neuroprotection after unilateral cervical spinal cord injury. *Spine.* 2010;35:2041–8.

3. Geissler J, Stevanovic M. Management of large peripheral nerve defects with autografting. *Injury*. 2019;50:S64–s67.
4. Behtaj S, Ekberg JAK, St John JA. Advances in electrospun nerve guidance conduits for engineering neural regeneration. *Pharmaceutics*. 2022;14:219.
5. Yang CY, Huang WY, Chen LH, Liang NW, Wang HC, Lu J, et al. Neural tissue engineering: the influence of scaffold surface topography and extracellular matrix microenvironment. *J Mater Chem B*. 2021;9:567–84.
6. Sarker MD, Naghieh S, McInnes AD, Schreyer DJ, Chen X. Regeneration of peripheral nerves by nerve guidance conduits: influence of design, biopolymers, cells, growth factors, and physical stimuli. *Prog Neurobiol*. 2018;171:125–50.
7. Boerboom A, Dion V, Chariot A, Franzen R. Molecular mechanisms involved in Schwann cell plasticity. *Front Mol Neurosci*. 2017;10:38.
8. Arthur-Farraj P, Coleman MP. Lessons from injury: how nerve injury studies reveal basic biological mechanisms and therapeutic opportunities for peripheral nerve diseases. *Neurotherapeutics*. 2021;18:2200–21.
9. Chen W, Wei ZR, Wu BH, Yang CL, Jin WH, Gong FY, et al. Effects of combined transplantation of rat Schwann cells and fibroblasts on nerve regeneration of denervated perforator flaps in rats and the mechanism. *Chinese journal of burns*. 2019;35:134–42.
10. Zigmund RE, Echevarria FD. Macrophage biology in the peripheral nervous system after injury. *Prog Neurobiol*. 2019;173:102–21.
11. Song L, Guo Q, Guo J, Xu X, Xu K, Li Y et al. Brachial plexus bridging with specific extracellular matrix modified chitosan/silk scaffold: a new expand of tissue engineered nerve graft. *J Neural Eng* 2022, 19, 026010.
12. Zheng T, Wu L, Sun S, Xu J, Han Q, Liu Y, et al. Coculture of Schwann cells and endothelial cells for synergistically regulating dorsal root ganglion behavior on chitosan-based anisotropic topology for peripheral nerve regeneration. *Burns Trauma*. 2022;10:tkac030.
13. Chen W, Ji L, Wei Z, Yang C, Chang S, Zhang Y, et al. miR-146a-3p suppressed the differentiation of hAMSCs into Schwann cells via inhibiting the expression of ERBB2. *Cell Tissue Res*. 2021;384:99–112.
14. Jones S, Eisenberg HM, Jia X. Advances and future applications of augmented peripheral nerve regeneration. *Int J Mol Sci*. 2016;17:1494.
15. Lotfi L, Khakbiz M, Moosazadeh Moghaddam M, Bonakdar S. A biomaterials approach to Schwann cell development in neural tissue engineering. *J Biomed Mater Res A*. 2019;107:2425–46.
16. Hopf A, Schaefer DJ, Kalbermatten DF, Guzman R, Madduri S. Schwann cell-like cells: origin and usability for repair and regeneration of the peripheral and central nervous system. *Cell*. 2020;9:1990.
17. Borlongan CV. Remyelinating the transected peripheral nerve by fabricated Schwann cells derived from bone marrow. *Exp Neurol*. 2010;225:243–5.
18. Ao Q, Fung CK, Tsui AY, Cai S, Zuo HC, Chan YS, et al. The regeneration of transected sciatic nerves of adult rats using chitosan nerve conduits seeded with bone marrow stromal cell-derived Schwann cells. *Biomaterials*. 2011;32:787–96.
19. Jiang L, Mee T, Zhou X, Jia X. Augmenting peripheral nerve regeneration with adipose-derived stem cells. *Stem Cell Rev Rep*. 2021;18:544–58.
20. Ching RC, Wiberg M, Kingham PJ. Schwann cell-like differentiated adipose stem cells promote neurite outgrowth via secreted exosomes and RNA transfer. *Stem Cell Res Ther*. 2018;9:266.
21. Chen W, Xiao S, Wei Z, Deng C, Nie K, Wang D. Schwann cell-like cells derived from human amniotic mesenchymal stem cells promote peripheral nerve regeneration through a MicroRNA-214/c-Jun pathway. *Stem Cells Int*. 2019;2019:2490761.
22. Jiang TM, Yang ZJ, Kong CZ, Zhang HT. Schwann-like cells can be induction from human nestin-positive amniotic fluid mesenchymal stem cells. *In vitro cellular & developmental biology Animal*. 2010;46:793–800.
23. Jung N, Park S, Choi Y, Park JW, Hong YB, Park HH, et al. Tonsil-derived mesenchymal stem cells differentiate into a Schwann cell phenotype and promote peripheral nerve regeneration. *Int J Mol Sci*. 2016;17:1867.
24. Martens W, Sanen K, Georgiou M, Struys T, Bronckaers A, Ameloot M, et al. Human dental pulp stem cells can differentiate into Schwann cells and promote and guide neurite outgrowth in an aligned tissue-engineered collagen construct in vitro. *FASEB J*. 2014;28:1634–43.
25. Huang Z, Powell R, Phillips JB, Haastert-Talini K. Perspective on Schwann cells derived from induced pluripotent stem cells in peripheral nerve tissue engineering. *Cell*. 2020;9:2497.
26. Liu CY, Yin G, Sun YD, Lin YF, Xie Z, English AW, et al. Effect of exosomes from adipose-derived stem cells on the apoptosis of Schwann cells in peripheral nerve injury. *CNS Neurosci Ther*. 2020;26:189–96.
27. Jiang L, Jones S, Jia X. Stem cell transplantation for peripheral nerve regeneration: current options and opportunities. *Int J Mol Sci*. 2017;18:94.
28. Yin L, Liu X, Shi Y, Ocansey DKW, Hu Y, Li X, et al. Therapeutic advances of stem cell-derived extracellular vesicles in regenerative medicine. *Cell*. 2020;9:707.
29. Rao F, Zhang D, Fang T, Lu C, Wang B, Ding X, et al. Exosomes from human gingiva-derived mesenchymal stem cells combined with biodegradable chitin conduits promote rat sciatic nerve regeneration. *Stem Cells Int*. 2019;2019:2546367.
30. Kalluri R, LeBleu VS. The biology, function, and biomedical applications of exosomes. *Science (New York, NY)*. 2020;367:eaau6977.
31. van Niel G, D'Angelo G, Raposo G. Shedding light on the cell biology of extracellular vesicles. *Nat Rev Mol Cell Biol*. 2018;19:213–28.
32. Zhou Y, Liu S, Zhao M, Wang C, Li L, Yuan Y, et al. Injectable extracellular vesicle-released self-assembling peptide nanofiber hydrogel as an enhanced cell-free therapy for tissue regeneration. *J Control Release*. 2019;316:93–104.
33. Lv K, Li Q, Zhang L, Wang Y, Zhong Z, Zhao J, et al. Incorporation of small extracellular vesicles in sodium alginate hydrogel as a novel therapeutic strategy for myocardial infarction. *Theranostics*. 2019;9:7403–16.
34. Pakulska MM, Ballios BG, Shoichet MS. Injectable hydrogels for central nervous system therapy. *Biomed Mater*. 2012;7:024101.
35. Francis NL, Bennett NK, Halikere A, Pang ZP, Moghe PV. Self-assembling peptide nanofiber scaffolds for 3-D reprogramming and transplantation of human pluripotent stem cell-derived neurons. *ACS biomaterials science & engineering*. 2016;2:1030–8.
36. Kleinman HK, Martin GR. Matrigel: basement membrane matrix with biological activity. *Semin Cancer Biol*. 2005;15:378–86.

37. Benton G, Arnaoutova I, George J, Kleinman HK, Koblinski J. Matrigel: from discovery and ECM mimicry to assays and models for cancer research. *Adv Drug Deliv Rev.* 2014;79–80: 3–18.
38. Martin J, Martinez J, Mehdi A, Subra G. Silicone grafted bioactive peptides and their applications. *Curr Opin Chem Biol.* 2019;52:125–35.
39. Singh S, Srivastava AK, Baranwal AK, Bhatnagar A, Das KK, Jaiswal S, *et al.* Efficacy of silicone conduit in the rat sciatic nerve repair model: journey of a thousand miles. *Neurol India.* 2021;69:318–25.
40. Braga Silva J, Marchese GM, Cauduro CG, Debiassi M. Nerve conduits for treating peripheral nerve injuries: a systematic literature review. *Hand Surg Rehabil.* 2017;36:71–85.
41. Chen W, Chang S, Yang C, Zhou J, Zhang H, Nie K, *et al.* Schwann cell-like cells derived from human amniotic mesenchymal stem cells promote sciatic nerve repair through an exosome-induced SOX2/FN1 pathway in vitro. *Int J Mol Med.* 2022;49:80.
42. Xian P, Hei Y, Wang R, Wang T, Yang J, Li J, *et al.* Mesenchymal stem cell-derived exosomes as a nanotherapeutic agent for amelioration of inflammation-induced astrocyte alterations in mice. *Theranostics.* 2019;9:5956–75.
43. Lopez-Verrilli MA, Picou F, Court FA. Schwann cell-derived exosomes enhance axonal regeneration in the peripheral nervous system. *Glia.* 2013;61:1795–806.
44. Huang B, Chen Z, Geng L, Wang J, Liang H, Cao Y, *et al.* Mucosal profiling of Pediatric-onset colitis and IBD reveals common Pathogenics and therapeutic pathways. *Cell.* 2019;179:1160–1176.e24.
45. Bain JR, Mackinnon SE, Hunter DA. Functional evaluation of complete sciatic, peroneal, and posterior tibial nerve lesions in the rat. *Plast Reconstr Surg.* 1989;83:129–36.
46. Wu P, Tong Z, Luo L, Zhao Y, Chen F, Li Y, *et al.* Comprehensive strategy of conduit guidance combined with VEGF producing Schwann cells accelerates peripheral nerve repair. *Bioact Mater.* 2021;6:3515–27.
47. Svaren J, Meijer D. The molecular machinery of myelin gene transcription in Schwann cells. *Glia.* 2008;56:1541–51.
48. Xie S, Lu F, Han J, Tao K, Wang H, Simental A, *et al.* Efficient generation of functional Schwann cells from adipose-derived stem cells in defined conditions. *Cell cycle (Georgetown, Tex).* 2017;16:841–51.
49. Chen J, Ren S, Duscher D, Kang Y, Liu Y, Wang C, *et al.* Exosomes from human adipose-derived stem cells promote sciatic nerve regeneration via optimizing Schwann cell function. *J Cell Physiol.* 2019;234:23097–110.
50. Yu M, Gu G, Cong M, Du M, Wang W, Shen M, *et al.* Repair of peripheral nerve defects by nerve grafts incorporated with extracellular vesicles from skin-derived precursor Schwann cells. *Acta Biomater.* 2021;134:190–203.
51. Lopez-Leal R, Court FA. Schwann cell exosomes mediate neuron-glia communication and enhance axonal regeneration. *Cell Mol Neurobiol.* 2016;36:429–36.
52. Wei Z, Fan B, Ding H, Liu Y, Tang H, Pan D, *et al.* Proteomics analysis of Schwann cell-derived exosomes: a novel therapeutic strategy for central nervous system injury. *Mol Cell Biochem.* 2019;457:51–9.
53. Cerqueira SR, Lee YS, Cornelison RC, Mertz MW, Wachs RA, Schmidt CE, *et al.* Decellularized peripheral nerve supports Schwann cell transplants and axon growth following spinal cord injury. *Biomaterials.* 2018;177:176–85.
54. Fouad K, Schnell L, Bunge MB, Schwab ME, Liebscher T, Pearse DD. Combining Schwann cell bridges and olfactory-ensheathing glia grafts with chondroitinase promotes locomotor recovery after complete transection of the spinal cord. *J Neurosci.* 2005;25:1169–78.
55. Meijis MF, Timmers L, Pearse DD, Tresco PA, Bates ML, Joosten EA, *et al.* Basic fibroblast growth factor promotes neuronal survival but not behavioral recovery in the transected and Schwann cell implanted rat thoracic spinal cord. *J Neurotrauma.* 2004;21:1415–30.
56. Jessen KR, Mirsky R. The repair Schwann cell and its function in regenerating nerves. *J Physiol.* 2016;594:3521–31.
57. Carr MJ, Johnston AP. Schwann cells as drivers of tissue repair and regeneration. *Curr Opin Neurobiol.* 2017;47: 52–7.
58. Zhou Y, Notterpek L. Promoting peripheral myelin repair. *Exp Neurol.* 2016;283:573–80.
59. Hoyng SA, De Winter F, Gnani S, de Boer R, Boon LI, Korvers LM, *et al.* A comparative morphological, electrophysiological and functional analysis of axon regeneration through peripheral nerve autografts genetically modified to overexpress BDNF, CNTF, GDNF, NGE, NT3 or VEGF. *Exp Neurol.* 2014;261:578–93.
60. Jin K, Zhu Y, Sun Y, Mao XO, Xie L, Greenberg DA. Vascular endothelial growth factor (VEGF) stimulates neurogenesis in vitro and in vivo. *Proc Natl Acad Sci U S A.* 2002;99: 11946–50.
61. Mokarram N, Merchant A, Mukhatyar V, Patel G, Bellamkonda RV. Effect of modulating macrophage phenotype on peripheral nerve repair. *Biomaterials.* 2012;33:8793–801.
62. Rosenstein JM, Krum JM, Ruhrberg C. VEGF in the nervous system. *Organ.* 2010;6:107–14.